INTER-ALGORITHM RELATIONSHIPS FOR RETRIEVALS OF FRACTION OF VEGETATION COVER IN A FRAMEWORK OF LINEAR MIXTURE MODEL

Kenta Obata[a] and Hiroki Yoshioka[a]

[a]Department of Information Science and Technology, Aichi Prefectural University
1522-3 Kumabari, Nagakute, Aichi, Japan
kenta.obata@cis.aichi-pu.ac.jp, yoshioka@ist.aichi-pu.ac.jp
Corresponding author's E-mail: yoshioka@ist.aichi-pu.ac.jp

KEY WORDS: Fraction of Vegetation Cover (FVC), Linear Mixture Model (LMM), Inter-Algorithm Relationship, Vegetation Index (VI), Error Propagation, Endmember.

ABSTRACT:

Fraction of vegetation cover (FVC) retrieved from remotely sensed reflectance spectra serves as a useful measure of land cover change. Since its retrieval algorithms show variations in assumptions of reflectance models and conditions imposed on the modeled spectra, the retrieved values also show some variations among the algorithms. This study discusses relationships among the FVC retrieval algorithms based on a well-known linear mixture model (LMM). The relationships among the algorithms were derived analytically within a framework of two-endmember LMM. It was clarified that some of the algorithms are equivalent in the sense that a one-to-one relationship exists among the algorithms. Numerical experiments had been conducted to evaluate the differences in error propagation among the algorithms induced by uncertainties in measured reflectance (often represented by a signal-to-noise ratio). The results indicate that the error propagation mechanisms are different in some extent among the algorithms. Moreover, the magnitude of the propagated error depends on the location of a target reflectance spectrum in the red-NIR reflectance space. Although the reflectance model employed in this study is quite limited, the fundamental aspects of the derived relationships would contribute to better understanding of the FVC retrievals.

1 INTRODUCTION

Vegetation plays an important role in various field of studies such as climatic, hydrologic, and geochemical cycles (Jiang et al., 2006). Biophysical parameters retrieved from satellite observations such as vegetation fraction and leaf area index also serve as a useful measure of land cover change (Jimenéz-Muñoz et al., 2009, Gutman and Ignatov, 1998). The focus of this study is a parameter which represents horizontal density, known as fraction of vegetation cover (FVC), widely used in application from local to global scale (Foody and Cox, 1994, Lobell et al., 2001).

Numerous algorithms have been proposed to retrieve FVC from remotely sensed reflectance spectrum. Those algorithms can be categorized into three based on level of dependency on numerical technique; (1) algorithms based on analytical formula (Shimabukuro and Smith, 1991, Xiao and Moody, 2005), in which numerical steps only appear in the final stage of retrieval process; (2) algorithms based on numerical model inversion of canopy radiative transfer (Huemmrich, 2001); and (3) algorithms using artificial intelligence such as neural networks (Carpenter et al., 1999). User can choose an algorithm based on their needs and objectives as well as availability of external data source.

In this study, we focus on the algorithms of the first category under in a framework of linear mixture model (LMM). Further variations of the algorithms within the same category arise by the differences in the assumptions and type of the model, the retrieved FVC can vary for a single spectrum (Chen et al., 2009). Several algorithms based on LMM have been utilized to retrieve FVC, however, relationship of FVC estimation between algorithms have not been clarified. The first objective of this study is to investigate the relationships among the retrieval algorithms based on LMM. The second objective is to compare the variances in FVC among the algorithms by modeling a certain degree of uncertainty in a target reflectance spectrum (often represented as a signal-to-noise ratio).

2 BACKGROUND

In a LMM, a measured reflectance spectrum can be represented by a linear sum of endmember spectra with a set of weights to be determined. The FVC retrieval algorithms in the framework of LMM show variations characterized by the choice of variables for endmember, conditions imposed on the model, and the number of endmember spectra and spectral bands. Those variations in the algorithms induce discrepancies in the estimated FVCs. We proceed our discussion based on a LMM with reflectance and spectral vegetation index (VI) as the variables. The number of endmembers and bands are both limited into two to proceed our discussion analytically. Two types of endmember, vegetation and non-vegetation, are assumed in this study. For example, the spectrum of the target pixel consist of red and NIR bands $\boldsymbol{\rho}_m$ is modeled by a weighted sum of vegetation and non-vegetation endmember ($\boldsymbol{\rho}_v = (\rho_{v,r}, \rho_{v,n})$ and $\boldsymbol{\rho}_s = (\rho_{s,r}, \rho_{s,n})$) as,

$$\boldsymbol{\rho}_m(\hat{\omega}) = \hat{\omega}\boldsymbol{\rho}_v + (1 - \hat{\omega})\boldsymbol{\rho}_s, \tag{1}$$

where $\hat{\omega}$ represents an estimated FVC. Note that the unity constraint is assumed in Eq.(1). Below, we introduce three algorithms based on the LMM with two-endmember assumption.

2.1 Algorithm-1: Reflectance-Based LMM

Reflectance-based LMM employs a reflectance spectrum as a endmember variable, and a set of weights for the endmembers (FVC) will be determined to minimize the difference between the modeled and measured reflectances (Shimabukuro and Smith, 1991). In general, root mean square error (RMSE) is used for minimization. In this case, the cost function can be considered as the distance between a target spectrum, $\boldsymbol{\rho}_t = (\rho_{t,r}, \rho_{t,n})$, and a modeled spectrum, $\boldsymbol{\rho}_m$. The FVC estimation, $\hat{\omega}$, is determined to minimize the distance,

$$\hat{\omega} = \frac{(\boldsymbol{\rho}_v - \boldsymbol{\rho}_s) \cdot (\boldsymbol{\rho}_t - \boldsymbol{\rho}_s)}{(\boldsymbol{\rho}_v - \boldsymbol{\rho}_s) \cdot (\boldsymbol{\rho}_v - \boldsymbol{\rho}_s)} = g_1(\boldsymbol{\rho}_t). \tag{2}$$

The FVC value retrieved by this algorithm is not the same as the one retrieved by the algorithms that use a VI as an additional condition, as explained in the following subsections.

2.2 Algorithm-2: VI-Based LMM

VI-based LMM uses VI as a endmember variable, and weights of endmember are determined to equate the modeled and measured VI (Gutman and Ignatov, 1998). Although numerous variations of the two-band VI (v) have been proposed, their forms can be represented by the function f,

$$\begin{aligned} v &= f(\boldsymbol{\rho}) \\ &= \frac{p_1\rho_r + q_1\rho_n + r_1}{p_2\rho_r + q_2\rho_n + r_2}, \end{aligned} \tag{3}$$

where the coefficients p_i, q_i, and r_i are determined by the chosen VI. For example, the normalized difference vegetation index (NDVI) (Rouse et al., 1974), difference vegetation index (DVI) (Tucker, 1979), perpendicular vegetation index (PVI) (Richardson and Wiegand, 1977), soil-adjusted vegetation index (SAVI) (Huete, 1988), transformed SAVI (TSAVI) (Baret and Guyot, 1991, Baret et al., 1989), and enhanced VI-2 (EVI2) (Jiang et al., 2008) can be represented by the above function. The coefficients for the VIs are summarized in Table.1.

Using the above function, reflectance spectrum measured by satellite sensor can be transformed to VI (v_t) by

$$v_t = f(\boldsymbol{\rho}_t). \tag{4}$$

Likewise, reflectance spectrum of endmember for vegetation and non-vegetation surface can be transformed to VI (v_v and v_s),

$$v_v = f(\boldsymbol{\rho}_v), \tag{5}$$
$$v_s = f(\boldsymbol{\rho}_s). \tag{6}$$

The modeled VI by VI-based LMM (v_m) can be represented as linear sum of v_v and v_s using the weight $\hat{\omega}$,

$$v_m(\hat{\omega}) = \hat{\omega}v_v + (1-\hat{\omega})v_s. \tag{7}$$

Then $\hat{\omega}$ is determined by imposing a condition such that modeled VI in Eq.(7) is equal to the VI obtained from a measured spectrum,

$$v_m(\hat{\omega}) = v_t. \tag{8}$$

Solving for $\hat{\omega}$, following equation can be obtained,

$$\hat{\omega} = \frac{v_t - v_s}{v_v - v_s}. \tag{9}$$

We define a function g_2 to represent the above transformation from v_t to $\hat{\omega}$ as

$$g_2(v_t) = \frac{v_t - v_s}{v_v - v_s}. \tag{10}$$

A general representation of the composite function becomes

$$\hat{\omega} = g_2(v_t) = (g_2 \circ f)(\boldsymbol{\rho}_t). \tag{11}$$

2.3 Algorithm-3: VI-isoline based LMM

VI-isoline based LMM uses a reflectance as an endmember, and weights of endmember are determined to equate the measured and modeled VI, which consist of red and NIR reflectance represented by a weighted sum of endmember spectra (Zhang et al., 2006).

VI-isoline based LMM models VI value using the function f based on a spectrum modeled by the LMM,

$$v_m(\hat{\omega}) = f(\boldsymbol{\rho}_m(\hat{\omega})), \tag{12}$$

where v_m represents the modeled VI. $\boldsymbol{\rho}_m$ is the spectrum modeled by the LMM with vegetation and non-vegetation endmember. Right hand side of Eq.(12) can be rewritten by

$$v_m(\hat{\omega}) = \frac{\boldsymbol{c}_1 \cdot \boldsymbol{\rho}_m(\hat{\omega}) + r_1}{\boldsymbol{c}_2 \cdot \boldsymbol{\rho}_m(\hat{\omega}) + r_2} \tag{13}$$

$$= \frac{\hat{\omega}\boldsymbol{c}_1 \cdot (\boldsymbol{\rho}_v - \boldsymbol{\rho}_s) + \boldsymbol{c}_1 \cdot \boldsymbol{\rho}_s + r_1}{\hat{\omega}\boldsymbol{c}_2 \cdot (\boldsymbol{\rho}_v - \boldsymbol{\rho}_s) + \boldsymbol{c}_2 \cdot \boldsymbol{\rho}_s + r_2}, \tag{14}$$

where the two vectors represented by $\boldsymbol{c}_i$ are defined as

$$\boldsymbol{c}_i = (p_i, q_i), \quad (i = 1, 2). \tag{15}$$

Then $\hat{\omega}$ is determined by imposing the condition used in the previous algorithm (VI-based LMM),

$$v_m(\hat{\omega}) = v_t. \tag{16}$$

The above equation can be solved for $\hat{\omega}$ to have

$$\hat{\omega} = \frac{(\boldsymbol{c}_1 - v_t\boldsymbol{c}_2) \cdot \boldsymbol{\rho}_s + r_1 - v_t r_2}{(v_t\boldsymbol{c}_2 - \boldsymbol{c}_1) \cdot (\boldsymbol{\rho}_v - \boldsymbol{\rho}_s)}. \tag{17}$$

We define a function g_3 to represent the above transformation from v_t to $\hat{\omega}$ as

$$g_3(v_t) = \frac{(\boldsymbol{c}_1 - v_t\boldsymbol{c}_2) \cdot \boldsymbol{\rho}_s + r_1 - v_t r_2}{(v_t\boldsymbol{c}_2 - \boldsymbol{c}_1) \cdot (\boldsymbol{\rho}_v - \boldsymbol{\rho}_s)}. \tag{18}$$

A general form of the above transformation becomes

$$\hat{\omega} = g_3(v_t) = (g_3 \circ f)(\boldsymbol{\rho}_t). \tag{19}$$

3 RELATIONSHIP BETWEEN ALGORITHMS

In this section, we describe the relationship of FVC estimation among the algorithms. If the relationship between two transformations is one-to-one (and onto), the FVC estimated by one algorithm can be transformed into the other uniquely. On contrary, if the relationship is not one-to-one, some degree of uncertainty would remain in the transformation. To further discuss the relationships, we differentiate the estimated FVC among the three algorithms by denoting them as $\hat{\omega}_1$, $\hat{\omega}_2$, and $\hat{\omega}_3$ for algorithm-1, -2, and -3, respectively.

3.1 Relationship Between Algorithm-1 and the Others

FVC estimation by algorithm-1 $\hat{\omega}_1$ is computed by the function g_1 for the target spectrum as

$$\hat{\omega}_1 = g_1(\boldsymbol{\rho}_t). \tag{20}$$

A single spectrum results in a single value of FVC by function g_1, however, the inverse function g^{-1} produces multiple spectra from a single value of FVC. We define a set of reflectance spectra that result in an identical value of $\hat{\omega}_1$ as $S_1(\hat{\omega}_1)$:

$$S_1(\hat{\omega}_1) = \{\boldsymbol{\rho} | g_1(\boldsymbol{\rho}) = \hat{\omega}_1\}. \tag{21}$$

A set of $\hat{\omega}_2$ that can be computed from $\boldsymbol{\rho} \in S_1(\hat{\omega}_1)$ are then defined by $T_{1\to2}(\hat{\omega}_1)$ as

$$T_{1\to2} = \{\hat{\omega}_2 |\ \hat{\omega}_2 = (g_2 \circ f)(\boldsymbol{\rho}),\ \boldsymbol{\rho} \in S_1(\hat{\omega}_1)\}. \tag{22}$$

Table 1: Coefficients of two-band VIs (p_i, q_i and r_i) used in this study.

	p_1	q_1	r_1	p_2	q_2	r_2
NDVI	-1	1	0	1	1	0
DVI	-1	1	0	0	0	1
PVI	$-a$ †	1	$-b$ †	0	0	$(1+a)^{1/2}$ †
SAVI	-1.5 *	1.5 *	0	1	1	0.5 *
TSAVI	$-a^2$ †	a †	$-ab$ †	1	a †	$-ab + X(1+a^2)$ †
EVI2	-2.5	2.5	0	2.4	1	1

* We assumed that $L = 0.5$.
† a and b represents the slope and intercept of a soil line. We also assumed that $X = 0.08$ in this study.

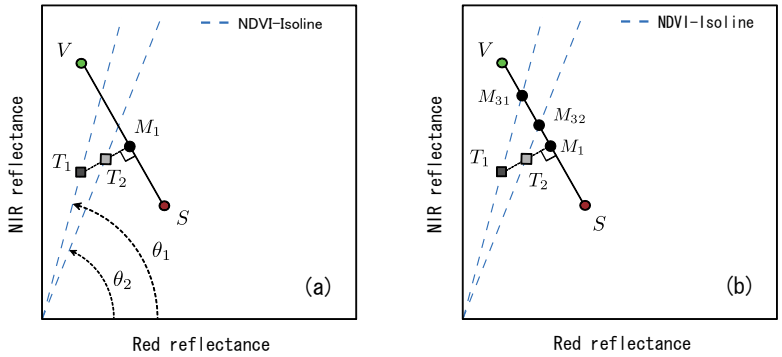

Figure 1: The relationship between algorithm-1 and the other two in red-NIR reflectance space, (a) for the relationship between algorithm-1 and -2, and (b) algorithm-1 and -3. V and S denote the endmember spectra of vegetation and non-vegetation classes. T_1 and T_2 are target spectra. M_1 is a modeled spectrum by algorithm-1 for the two target spectra which are identical in this example. M_{31} and M_{32} denote modeled spectra by algorithm-3 for the two targets. The figures illustrate the source of uncertainties between those algorithms.

Similarly, the relationship among algortithm-1 and -3 can be represented by defining $T_{1\to3}$ as

$$T_{1\to3} = \{\hat{\omega}_3 |\ \hat{\omega}_3 = (g_3 \circ f)(\boldsymbol{\rho}),\ \boldsymbol{\rho} \in S_1(\hat{\omega}_1)\}. \tag{23}$$

Since these mappings ($T_{1\to2}$ and $T_{1\to3}$) are not one-to-one, the relationship between $\hat{\omega}_1$ and the others ($\hat{\omega}_2$ and $\hat{\omega}_3$) are not uniquely determined. The relationships are illustrated in Fig. 1. In the figure, NDVI is chosen for algorithm-2 and -3 as the endmember or the conditions to determine FVC. Figure 1a shows the relationship between algorithm-1 and -2 in the red-NIR reflectance space. T_1 and T_2 denote different target spectra, and V and S denote vegetation and non-vegetation endmembers, respectively. The variable θ_1 and θ_2 are the angles between the NDVI-isolines which go though the target spectra (T_1 and T_2) and x-axis. T_1 and T_2 result in an identical FVC value by algorithm-1 because the closest point (M_1) in the model subspace is the same. On the other hand, since θ_1 and θ_2 are not the same value, the estimated FVCs from the two spectra are different. Similarly, the relationship between algorithm-1 and -3 is illustrated in Fig. 1b. Although algorithm-1 produces the same value of FVC from T_1 and T_2, the FVCs obtained by algorithm-3 are different illustrated as the different points (M_{31} and M_{32}) on one dimensional subspace spanned between V and S. In consequence, the FVC retrieved by algorithm-1 is not transformed to a single value of FVC by algorithm-2 and -3.

3.2 Relationship Between Algorithm-2 and -3

The relationship between these algorithms becomes one-to-one, that is, results by one algorithm can be transformed to the other uniquely. The one-to-one relationship can be obtained to relate formulation of each algorithm using VI computed from measured reflectance, v_t, which exists in both algorithms. FVC estimation by algorithm-2 can be obtained directly from v_t as

$$\hat{\omega}_2 = g_2(v_t), \tag{24}$$

Likewise, FVC estimation by algorithm can be written as follows,

$$\hat{\omega}_3 = g_3(v_t). \tag{25}$$

Solving Eq.(24) for v_t using the inverse function of g_2^{-1} gives

$$v_t = g_2^{-1}(\hat{\omega}_2). \tag{26}$$

A relationship between $\hat{\omega}_2$ and $\hat{\omega}_3$ can be defined as a composite function by substituting Eq.(26) into Eq.(25),

$$\hat{\omega}_3 = (g_3 \circ g_2^{-1})(\hat{\omega}_2). \tag{27}$$

Similarly, $\hat{\omega}_2$ can be written as a function of $\hat{\omega}_3$.

$$\hat{\omega}_2 = (g_2 \circ g_3^{-1})(\hat{\omega}_3). \tag{28}$$

Since both g_2 and g_3 are one-to-one transformations, $\hat{\omega}_2$ and $\hat{\omega}_3$ in Eq.(27) has one-to-one relationship. (The same goes to Eq.(28) as well.) The actual form of Eq.(27) becomes

$$\hat{\omega}_3 = \frac{(\phi + \psi)\hat{\omega}_2}{\phi\hat{\omega}_2 + \psi}, \tag{29}$$

where

$$\phi = (v_v - v_s)\boldsymbol{c}_2 \cdot (\boldsymbol{\rho}_v - \boldsymbol{\rho}_s) \tag{30a}$$
$$\psi = (v_s\boldsymbol{c}_2 - \boldsymbol{c}_1) \cdot (\boldsymbol{\rho}_v - \boldsymbol{\rho}_s). \tag{30b}$$

Note that this relationship can be obtained if and only if the choice of VI in both algorithm-2 and -3 are equivalent. Thus the relation-

Table 2: Summary of ϕ and ψ for the VIs considered in this study. $\rho_{v,r}$ and $\rho_{v,n}$ are the red and NIR reflectance of vegetation endmember, respectively. Likewise, $\rho_{s,r}$ and $\rho_{s,n}$ are the red and NIR reflectance of non-vegetation endmember, respectively. a represents a slope of soil line.

	ϕ	ψ
NDVI	$(v_v - v_s)(\rho_{v,r} + \rho_{v,n} - \rho_{s,r} - \rho_{s,n})$	$(1+v_s)(\rho_{v,r} - \rho_{s,r}) - (1-v_s)(\rho_{v,n} - \rho_{s,n})$
DVI	0	$\rho_{v,r} - \rho_{v,n} - \rho_{s,r} + \rho_{s,n}$
PVI	0	$a(\rho_{v,r} - \rho_{s,r}) - \rho_{v,n} + \rho_{s,n}$
SAVI	$(v_v - v_s)(\rho_{v,r} + \rho_{v,n} - \rho_{s,r} - \rho_{s,n})$	$(1.5+v_s)(\rho_{v,r} - \rho_{s,r}) - (1.5-v_s)(\rho_{v,n} - \rho_{s,n})$
TSAVI	$(v_v - v_s)[\rho_{v,r} - \rho_{s,r} + a(\rho_{v,n} - \rho_{s,n})]$	$(a^2+v_s)(\rho_{v,r} - \rho_{s,r}) + a(v_s-1)(\rho_{v,n} - \rho_{s,n})$
EVI2	$(v_v - v_s)[2.4(\rho_{v,r} - \rho_{s,r}) + \rho_{v,n} - \rho_{s,n}]$	$(2.4v_s+2.5)(\rho_{v,r} - \rho_{s,r}) + (v_s-2.5)(\rho_{v,n} - \rho_{s,n})$

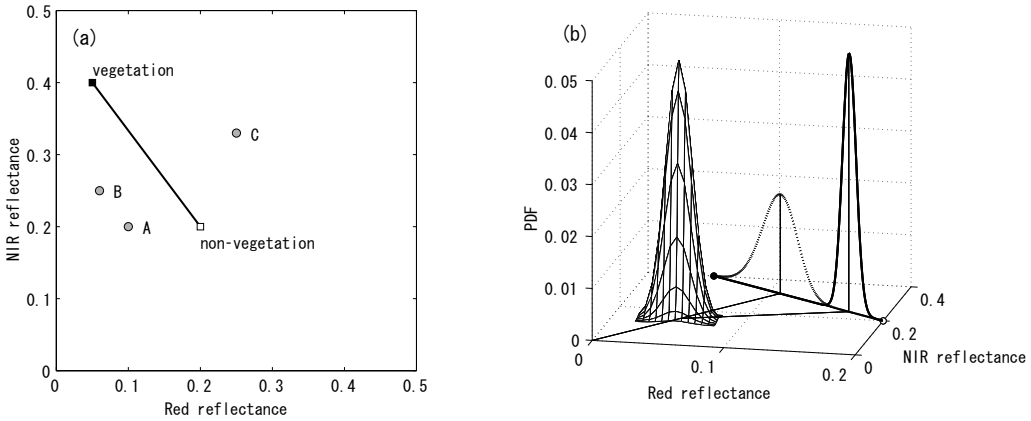

Figure 2: Illustration of the numerical experiment for FVC errors induced by uncertainties in observed reflectance spectrum. (a) Three target spectra (A, B, and C,) and endmember spectra of vegetation (filled square) and non-vegetation (empty square) in the reflectance space. (b) Illustration about error propagation in the FVC retrievals. The two-parameter normal distribution represents measurement uncertainties which are projected over the modeled subspace (the line between the two endmember spectra).

ship depends on the choice of VI as well as the endmember spectra of vegetation and non-vegetation surfaces. The forms of the coefficients ϕ and ψ for several VIs are summarized in Table.2.

4 BIASED FVC AND THEIR RELATIONSHIP BETWEEN ALGORITHMS INDUCED BY UNCERTAINTIES OF MEASUREMENTS

4.1 FVC Errors Induced by Uncertainties in an Observed Reflectance Spectrum

Numerical experiments had been conducted to compare the errors in retrieved FVC induced by the uncertainties of a target spectrum among the algorithms (often represented as a signal-to-noise ratio). The algorithms-1 and -3 were compared by employing five different VIs (NDVI, DVI, SAVI, TSAVI, and EVI2) as a condition for algorithm-3.

The spectra denoted by the filled and empty squares in the red-NIR reflectance space (Fig. 2a) represent the vegetation and the non-vegetation endmembers, respectively, which are connected by a solid line which represents a model space of the two-endmember LMM. The two-parameter Gaussian distribution (Fig. 2b) was assumed as a function of error distribution around the three targets spectra denoted by A, B, and C in Fig. 2a. The spectra of the three targets (A, B, and C in Fig. 2a) are $A = (0.1, 0.2)$, $B = (0.06, 0.25)$, and $C = (0.25, 0.33)$.

The expected values of FVC for the three target spectra are computed based on the error distribution function around the target spectra for algorithm-1 and -3. Figure 3a is the FVC distribution by the algorithm-1. The corresponding FVC distributions by algorithm-3 are plotted in Figs. 3(b-f) with a condition of NDVI, DVI, SAVI, TSAVI and EVI2, respectively. Those figures clearly show the differences in the distributions of estimated FVC among the algorithms. The differences are prominent for the DVI case (Fig. 3c): The distributions for the target spectra of A and C become in a different order than the other cases. (The distribution for the spectrum A is smaller than that for C in (c), while the distribution for the spectrum C becomes smaller than that for A in the others.) These results also imply that the variance in FVC distribution will be different among the choice of VI in algorithm-3 (as a condition for FVC determination.) To investigate this point, we further conducted a numerical experiment explained in the next subsection.

4.2 Relationship of Biased FVC Between Algorithms

The relationships of error propagation on estimated FVCs among the algorithms are examined numerically. In the previous subsection we assumed two-parameter Gaussian distribution as a probability distribution function (PDF) to represent uncertainty around a target spectrum. In this subsection, we assumed one-parameter Gaussian distribution along a line which goes through a target spectrum as illustrated in Fig. 4. The center of the Gaussian distribution is located at the target spectrum in the red-NIR reflectance space. The line of distribution (red solid line in Fig. 4) which goes through the point of the target spectrum in the reflectance space had been rotated 180 degrees around the point of the target spectrum. The variance of FVC distribution by the three different algorithms (algorithm-1, algorithm-3 with NDVI as a condition, and algorithm-3 with SAVI as a condition) were computed at each angle. Thus, we obtained three set of variances as a function of the angle.

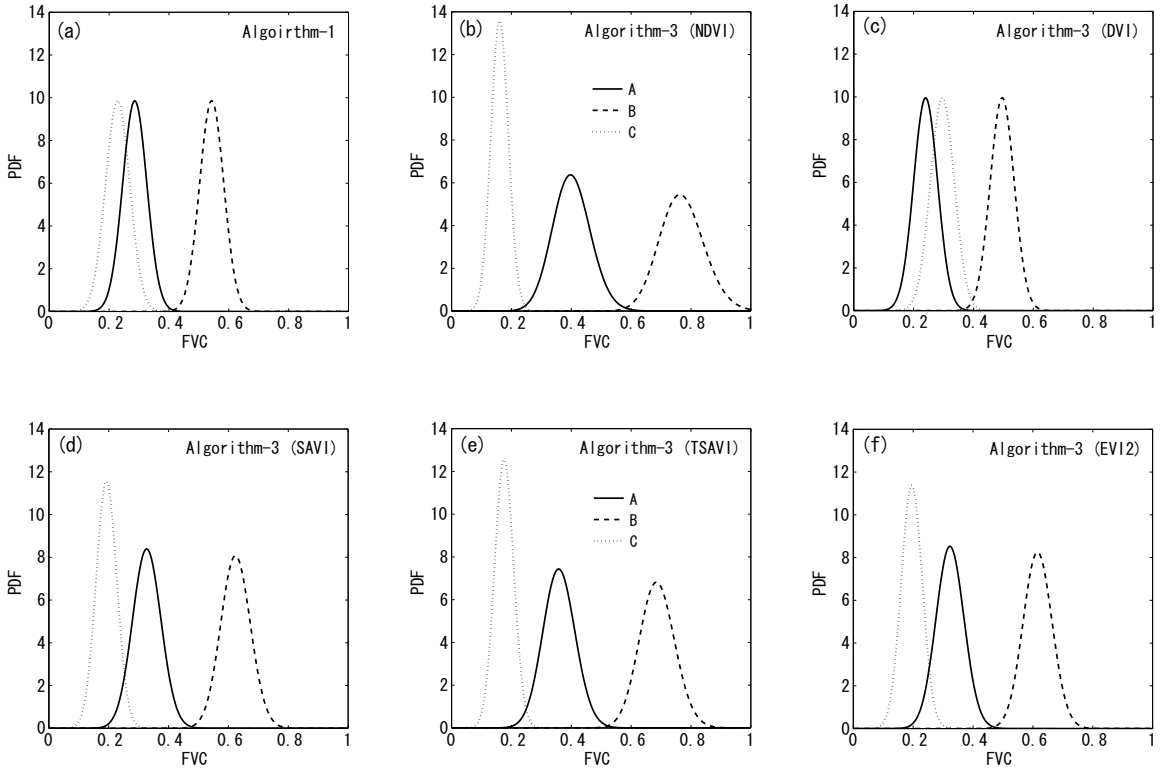

Figure 3: Distribution of the FVC estimations for the three target spectra which include uncertainties. Figure (a) show the results of FVC distributions by algorithm-1. Figures (b) through (f) are the results by algorithm-3 using NDVI, DVI, SAVI, TSAVI, and EVI2, respectively.

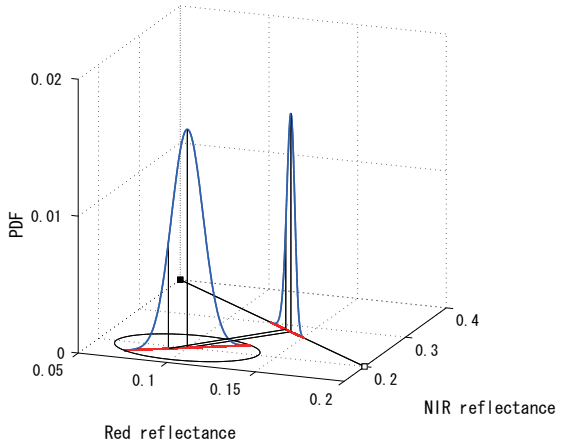

Figure 4: Illustration of the numerical experiments to examine the relationships of the variances in FVC among the algorithms. The variances of the FVC estimations were obtained by projecting the one-parameter normal distribution onto the model subspace spanned by the two endmember spectra. The axis of the normal distribution of the target spectra (red line) were rotated 180 degrees around the average spectrum.

Figures 5(a-c) show the relationships of variance among the three algorithms. From those figures the variance relationships depend on the choice of the algorithms as well as the VI as a condition for algorithm-3. The results also indicate that the variance relationships depends on the target spectra (denoted by A, B, and C.)

In general, each algorithm has advantage and disadvantage over the other algorithms regarding the robustness against uncertainties in an observed reflectance spectrum. The relationships among the algorithm (strength and weakness) depends on the location of the target spectra in the red-NIR reflectance space. When a target spectrum is located in lower region of the reflectance space relative to the model subspace (the line connecting the two endmember spectra), the parallel based LMM is less influenced by the uncertainties of measurement (hence robust to it) than the angle based LMM. On contrary, when a target spectrum is located in upper region of the reflectance space relative to the model subspace, the angle based LMM is more robust than the parallel based LMM.

5 DISCUSSION AND CONCLUSIONS

The relationships among the FVC retrieval algorithms were derived in a framework of two-endmember LMM. One to one relationships was successfully derived between the algorithms using the same vegetation index as a condition of FVC determination. This analytical investigation imply the difference in error of FVC induced by an uncertainty in a measurement.

The error propagation from a measured spectrum to FVC estimations by LMM based retrieval algorithms was numerically simulated under a two-endmember assumption. It was shown that the amplitudes of biases strongly depend on a target reflectance spectrum (represented as a position in the red-NIR reflectance space). The results indicate that both average and standard deviation of the FVC estimations are different among the algorithms for an identical target spectrum (the probability distribution function of the target spectrum). It implies that much caution is needed to choose an algorithm and its condition for the FVC determinations. The results also imply that the variance in FVC estimation

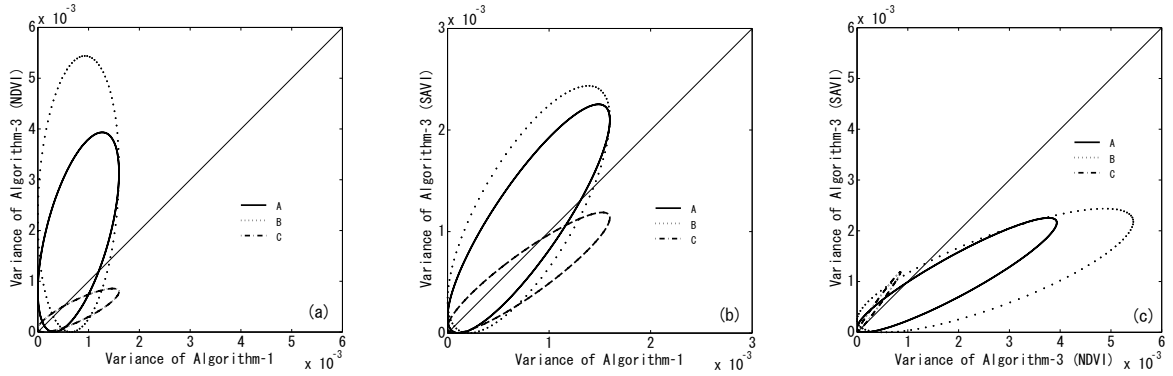

Figure 5: Relationships of the FVC variances among the algorithms for the three targets. The relationship between (a) algoirthm-1 and algorithm-3 using NDVI; (b) algorithm-1 and algorithm-3 using SAVI; and (c) algorithm-3 using NDVI and algorithm-3 using SAVI.

show a systematic difference among the algorithms. We then investigate the relationship of variance in FVC estimations among the retrieval algorithms to clarify the relationships of variance among the algorithms. The results clearly show the existence of such relationships among the algorithms.

In this study we employed the simplest model among the LMMs to proceed the investigation analytically. Although the results obtained in this study cannot be applicable to more complicated cases (e.g. multiple-endmember LMM), the findings must have some degree of generality which would serve as a theoretical basis in some extent for the estimation of vegetation fraction from satellite images.

REFERENCES

Baret, F. and Guyot, G., 1991. Potentials and limits of vegetation indices for LAI and APAR assessment. Remote Sens. Environ. 35, pp. 161–173.

Baret, F., Guyot, G. and Major, D., 1989. Tsavi: A vegetation index which minimizes soil brightness effects on lai and apar estimation. In: Geosci. and Remote Sens. Symp., 1989. IGARSS'89. 12th Can. Symp. on Remote Sens., 1989 International, Vol. 3, pp. 1355–1358.

Carpenter, G. A., Gopal, S., Macomber, S., Martens, S. and Woodcock, C. E., 1999. A neural network method for mixture estimation for vegetation mapping. Remote Sens. Environ. 70, pp. 138–152.

Chen, J., Jia, X., Yang, W. and Matsushita, B., 2009. Generalization of subpixel analysis for hyperspectral data with flexibility in spectral similarity measures. IEEE Trans. Geosci. Remote Sens. 47(7), pp. 2165–2171.

Foody, G. M. and Cox, D. P., 1994. Sub-pixel land cover composition estimation using a linear mixture model and fuzzy membership functions. Int. J. Remote Sens. 15(3), pp. 619–631.

Gutman, G. and Ignatov, A., 1998. The derivation of the green vegetation fraction from NOAA/AVHRR data for use in numerical weather prediction models. Int. J. Remote Sens. 19(8), pp. 1533–1543.

Huemmrich, K. F., 2001. The GeoSail model: a simple addition to the SAIL model to describe discontinuous canopy reflectance. Remote Sens. Environ. 75, pp. 423–431.

Huete, A. R., 1988. A soil-adjusted vegetation index (SAVI). Remote Sens. Environ. 25, pp. 295–309.

Jiang, Z., Huete, A. R., Chen, J., Chen, Y., Li, J., Yan, G. and Zhang, X., 2006. Analysis of NDVI and scaled difference vegetation index retrievals of vegetation fraction. Remote Sens. Environ. 101, pp. 366–378.

Jiang, Z., Huete, A. R., Didan, K. and Miura, T., 2008. Development of a two-band enhanced vegetation index without a blue band. Remote Sens. Environ. 112, pp. 3833–3845.

Jimenéz-Muñoz, J. C., Sobrino, J. A., Plaza, A., Guanter, L., Moreno, J. and Martinez, P., 2009. Comparison between fractional vegetation cover retrievals from vegetation indices and spectral mixture analysis: case study of PROBA/CHRIS data over an agricultural area. Sensors 9, pp. 768–793.

Lobell, D. B., Asner, G. P., Law, B. E. and Treuhaft, R. N., 2001. Subpixel canopy cover estimation of coniferous forests in Oregon using SWIR imaging spectrometry. J. Geophys. Res. 106(6), pp. 5151–5160.

Richardson, A. J. and Wiegand, C. L., 1977. Distinguishing vegetation from soil background information (by gray mapping of Landsat mss data). Photogramm. Eng. Remote Sens. 43(12), pp. 1541–1552.

Rouse, J. W., Haas, R. H., Schell, J. A. and Deering, D. W., 1974. Monitoring vegetation systems in the great plains with ERTS. in Proc. 3rd ERTS Symp., NASA SP-351, Washington, DC, Dec. 10-14 pp. 309–317.

Shimabukuro, Y. E. and Smith, J. A., 1991. The least-squares mixing models to generate fraction images derived from remote sensing multispectral data. IEEE Trans. Geosci. Remote Sens. 29(1), pp. 16–20.

Tucker, C. J., 1979. Red and photographic infrared linear combinations for monitoring vegetation. Remote Sens. Environ. 8, pp. 127–150.

Xiao, J. and Moody, A., 2005. A comparison of methods for estimating fractional green vegetation cover within a desert-to-upland transition zone in central New Mexico, USA. Remote Sens. Environ. 98, pp. 237–250.

Zhang, X., Yan, G., Li, Q., Li, Z.-L., Wan, H. and Guo, Z., 2006. Evaluating the fraction of vegetation cover based on NDVI spatial scale correction model. Int. J. Remote Sens. 27(23-24), pp. 5359–5372.